ELSEVIER

Thermochimica Acta 398 (2003) 131–143

thermochimica acta

www.elsevier.com/locate/tca

Comparative study of the thermal and redox behaviour of alkali-promoted V_2O_5 catalysts

Ursula Bentrup*, Andreas Martin, Gert-Ulrich Wolf

Institut für Angewandte Chemie Berlin-Adlershof e.V., Richard-Willstätter Street 12, D-12489 Berlin, Germany

Received 16 January 2002; received in revised form 23 May 2002; accepted 27 May 2002

Abstract

Alkali-promoted V_2O_5 catalysts M-V_2O_5 (M = Li, Na, K, Rb and Cs) synthesised by impregnation of V_2O_5 with alkali sulfate solution have been investigated under inert and reducing atmosphere using thermoanalytical methods (TG/DTA, differential scanning calorimetry (DSC) and temperature-programmed reduction (TPR)). Pure V_2O_5 was used for comparison. Whereas in Li- and Na-promoted catalysts only V_2O_5 as crystalline phase could be detected by X-ray diffraction (XRD), the K-, Rb-, and Cs-promoted catalysts additionally contain the vanadate phase MV_3O_8. The surface acidity (Brønsted- and Lewis-sites) as well as the starting temperature of the hydrogen consumption decrease with increasing size of the alkali cation. The reduction of the K-, Rb-, and Cs-promoted catalysts leads to the formation of bronze-like phases besides V_2O_5 at relative low temperatures. The bronze phases stabilise the V^{4+} oxidation state and improve the redox properties. A characteristic splitting and shifting of the ν(V=O) mode in the FTIR spectrum indicates the formation of V^{4+} in the different bronze phases. The favoured formation of bronze-like phases especially under reducing conditions enhances the release of SO_2 at lower temperatures, the formation of H_2S can be neglected.

Keywords: V_2O_5 catalysts; Vanadate phases; Bronze phases; Thermal analysis; FTIR; XRD

1. Introduction

Vanadium oxide (V_2O_5) catalysts have been widely used in partial oxidation reactions [1]. The promotion of V_2O_5 with alkali compounds or basic oxides and their effect for catalytic performance in different reactions has been the subject of several studies [2–9]. Generally, the promotion of V_2O_5 bulk and supported catalysts with alkali compounds improves the selectivity to partial oxidation products.

Mainly Japanese groups reported on the role of acid and base properties of vanadium oxide catalysts containing basic metal oxides (M = K, Rb, Cs, Tl and Ag) for the partial oxidation of methyl aromatics to their corresponding aldehydes [3,4]. They stated that the selectivity to substituted benzaldehydes is closely related to the basic properties of the catalyst whereas the activity strongly depends on the amount and strength of acid sites. Ponzi et al. [5] showed that the catalyst activity for the partial oxidation of toluene decreases in the order $V_2O_5 > V_2O_5$-K > V_2O_5-K-SiO_2, whereas the selectivities for partial oxidation products show the opposite trend. They assumed a lowering of the number of acid sites by addition of K_2SO_4 to the V_2O_5 catalyst. Monti et al. [2] investigated the relationship between the reduction behaviour and the structure of K_2SO_4-promoted V_2O_5 catalysts and their activity and selectivity using the partial oxidation of methanol to formaldehyde as model reaction. They found that

* Corresponding author. Fax: +49-30-6392-4350.
E-mail address: bentrup@aca-berlin.de (U. Bentrup).

0040-6031/03/$ – see front matter
PII: S0040-6031(02)00334-9

the selectivities for formaldehyde were higher for all catalysts containing K_2SO_4. Additionally, the starting temperatures for catalyst reduction by hydrogen were lowered in dependence on concentration of K_2SO_4.

The potassium doping effect was also investigated during selective toluene oxidation to benzaldehyde on V_2O_5/TiO_2 catalysts [8]. The addition of potassium leads to an increased formation of benzaldehyde. The authors concluded that potassium addition causes a lower surface concentration of electrophilic oxygen, which is responsible for deep oxidation and a higher concentration of nucleophilic oxygen responsible for the partial oxidation. Furthermore, they found that potassium addition introduces a disorder in the crystalline structure of bulk V_2O_5 particles resulting in better spreading of V_2O_5 over the TiO_2 surface.

Tarama et al. [10] investigated the properties of the V_2O_5–K_2SO_4 system and explained the promoter action of K_2SO_4 by a weakening of the V=O bond in the V_2O_5 lattice. Additionally, they found a lowering of the melting point of the mixed catalysts. A lowering of the melting points of mixed oxide catalysts containing vanadium and alkali cations was also reported in [3,4] and it was closely related to the formation of different alkali vanadate phases.

Recent studies of the partial oxidation of substituted toluene to their corresponding aldehydes on alkali metal-containing V_2O_5 catalysts have shown that toluene conversion and aldehyde selectivity change with alkali cation size [9]. Increasing cation size and consequently increasing basicity in the order from Li to Cs causes declining toluene conversion but increasing aldehyde selectivity. The best aldehyde selectivities were observed for the K-V_2O_5 and Cs-V_2O_5 catalysts. Vanadate and bronze phases of the more bulky alkali metal cations (K, Rb and Cs) are generated during catalyst synthesis and catalytic reaction. It was assumed that such phases favour new surface arrangements with V_2O_5 and influence the catalytic activity. Incorporation of the smaller lithium and sodium cations does not lead to the formation of vanadate and bronze phases.

Summarising the various investigations of mainly potassium doped V_2O_5 catalysts, it can be concluded that both, the surface acidity/basicity and the redox properties of such catalysts are influenced by alkali admixture. But, no comparative and systematic studies of modified V_2O_5 catalysts are known including different alkali metals in comparable concentrations.

In this study, the thermal behaviour, the redox properties and the phase changes of V_2O_5 catalysts modified with alkali sulfate will be compared using thermoanalytical methods, XRD and FTIR spectroscopy.

2. Experimental

2.1. Catalyst preparation

M-V_2O_5 catalysts were prepared by the incipient wetness method with an aqueous M_2SO_4 (M = Li, Na, K, Rb and Cs) solution. Measured 50 ml of such a solution (0.01 mol M_2SO_4) was added to V_2O_5 (0.1 mol) and evaporated using a rotary evaporator at 70 °C for 1 h. A further evaporation to dryness was carried out under vacuum at this temperature. The obtained product was dried overnight at 130 °C. For comparison, pure V_2O_5 was treated by the same procedure using distilled water.

Additionally, KV_3O_8 was synthesised according to a method described by Kelmers [11]. A total of 45.49 g (0.25 mol) V_2O_5 was introduced stepwise into a solution of 28.14 g (0.5 mol) KOH in 500 ml distilled water during 30 min. For complete oxidation of vanadium 3 ml H_2O_2 (30%) was added. After filtration, the solution was heated up to 80 °C under vigorous stirring and 20.5 g (ca. 0.2 mol) H_2SO_4 were slowly added. The orange-brown solid was further stirred for 72 h at 80 °C, then filtered, washed and dried.

2.2. Catalyst characterisation

The obtained samples were characterised by X-ray diffraction (XRD) using an automatic transmission powder diffractometer (Stoe STADI P) and FTIR spectroscopy (Mattson Galaxy 5020) using the KBr technique.

The surface areas were determined by N_2-physisorption using the BET method (Gemini III 2375, Micromeritics). The samples (ca. 0.5–1.0 g) were pre-treated at 150–200 °C for 1h under vacuum. The acidic properties were estimated by FTIR spectroscopy using pyridine as probe molecule. For the adsorption experiments, the catalyst powders were

pressed into self-supporting disks with a diameter of 20 mm and a weight of 50 mg. Prior to the adsorption of pyridine at room temperature the catalysts were pre-treated in the IR cell by heating in Ar up to 300–400 °C followed by cooling down to adsorption temperature. The spectra were recorded by means of a Bruker IFS 66 spectrometer.

Temperature-programmed reduction (TPR) measurements were carried out on AMI-1 equipment (Altamira/Zeton). For the experiments the samples (12–16 mg) were heated in 5 vol.% H_2/Ar (3 l/h) with a heating rate of 10 K/min and an isothermal hold at the final temperature of 900 °C for 30 min. Water formed or desorbed during measurements was removed by molecular sieve 4A before the flow passed the thermal conductivity detector (TCD).

2.3. Thermal analysis

Thermal analytical measurements (TG, DTA) were carried out on a Netzsch STA 409 thermoanalyser connected by a heated stainless steel capillary to a Balzers quadrupole mass spectrometer QMG 420.

For the standard experiments, the samples (50–60 mg) were heated (5 °C/min) in He or 5 vol.% H_2/Ar (3 l/h) using Al_2O_3 crucibles, the reference material was Al_2O_3. Differential scanning calorimetric (DSC) measurements were performed using a DSC-7 instrument (Perkin-Elmer). The samples (12–25 mg) were heated (10 °C/min) in Ar (1.6 l/h) using closed and perforated Al pans.

3. Results and discussion

3.1. Characterisation of the catalysts

Table 1 presents the phase composition determined by XRD and the surface area of the prepared alkali promoted catalysts. In the case of K-V_2O_5, Rb-V_2O_5, and Cs-V_2O_5 a crystalline phase M-V_3O_8 was formed in addition to V_2O_5. No formation of $5V_2O_5{\cdot}3K_2SO_4$ was observed as described in [2].

Table 1
Phase composition and BET surface areas of the parent catalysts

Catalyst	Phase composition	S_{BET} (m^2/g)
Li-V_2O_5	V_2O_5	7.22
Na-V_2O_5	V_2O_5	6.52
K-V_2O_5	V_2O_5, KV_3O_8	5.18
Rb-V_2O_5	V_2O_5, RbV_3O_8	6.07
Cs-V_2O_5	V_2O_5, CsV_3O_8	4.69

For the comparative studies in addition to V_2O_5 mainly Li-V_2O_5, K-V_2O_5 and Cs-V_2O_5 were used. The investigation of Na-V_2O_5 and Rb-V_2O_5 has been omitted because of the structural similarities with the respective Li- and K-promoted catalysts.

For characterising the surface acidity, pyridine was adsorbed at room temperature. The FTIR spectra obtained after adsorption of pyridine and following evacuation for V_2O_5, Li-V_2O_5, and Cs-V_2O_5 are depicted in Fig. 1. The bands which characterise Lewis- and Brønsted-acidic sites are assigned in the figure. It is clearly seen that alkali-promotion influences the number of such sites. Especially the number of Brønsted-sites strongly decreases with increasing size of the alkali cation. In the case of caesium also the Lewis-sites are diminished.

The TPR curves measured for V_2O_5, Li-V_2O_5, K-V_2O_5, and Cs-V_2O_5 are presented in Fig. 2. The reduction profiles are different and point to a complicated reduction behaviour. The beginning of the hydrogen consumption is lowered from 667 °C for the pure V_2O_5 catalyst to approximately 463 °C for Cs-V_2O_5. Obviously, the starting point of hydrogen consumption drops with increasing size of the promoted alkali cation. The total hydrogen consumption calculated by peak integration within the whole temperature range up to 900 °C gives hydrogen uptakes (referred to the vanadium content) ranging from 5.75 mmol/g for V_2O_5, 4.69 mmol/g for Li-V_2O_5, 4.37 mmol/g for K-V_2O_5 to 4.01 mmol/g for Cs-V_2O_5. That means, alkali-promotion influences the reduction degree in a different way. Compared with the hydrogen uptake of pure V_2O_5, a lowering of the reduction degree has been observed. This effect can be explained with the stabilisation of V^{4+} by formation of special vanadate phases which are more stable against reduction.

3.2. Thermal behaviour in inert and reducing atmosphere

Comparing the thermal behaviour of the catalysts in inert atmosphere with that under reducing conditions some essential differences have been observed. The TG and DTA curves obtained in He and H_2/Ar

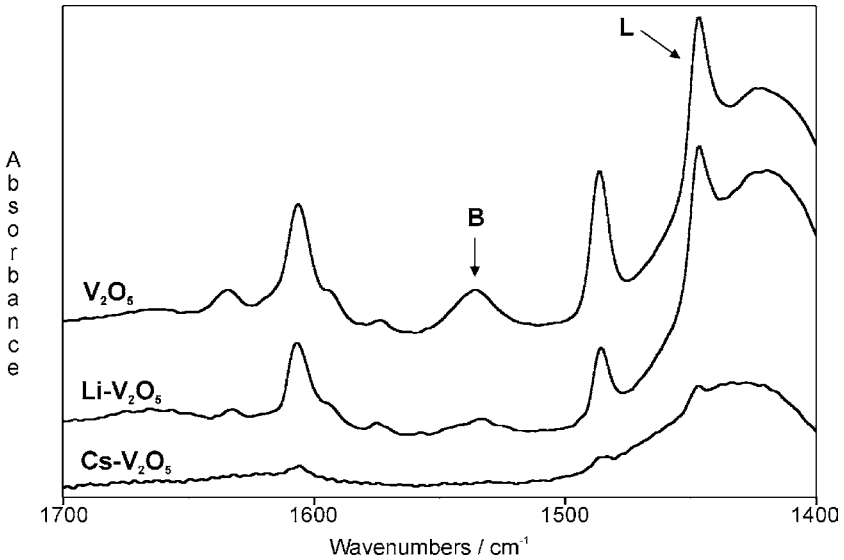

Fig. 1. FTIR spectra of pyridine adsorbed at room temperature on V_2O_5, Li-V_2O_5, and Cs-V_2O_5 (B: Brønsted-sites; L: Lewis-sites).

atmosphere are shown for V_2O_5, Li-V_2O_5, K-V_2O_5, and Cs-V_2O_5 in Fig. 3. The low temperature range (evolution of adsorbed water) is omitted for more clarity. The mass losses and the temperatures of the DTG and the endothermic DTA peaks calculated from the TG and DTA curves (Fig. 3) for the different catalysts, respectively, are summarised in Table 2.

In contrast to pure V_2O_5 in the temperature range of 550–700 °C, a significant mass loss is observed in inert atmosphere for all alkali-promoted catalysts (Fig. 3A). Furthermore, in reducing atmosphere, the beginning of the mass loss is shifted to lower temperatures (Fig. 3B, Table 2). This effect is more pronounced in the case of K-V_2O_5 and Cs-V_2O_5 than for Li-V_2O_5. A significant mass loss was also found for pure V_2O_5 above 650 °C pointing to the beginning reduction. The DTA curves show great differences in dependence on the ambient atmosphere. Under inert atmosphere only one major endothermic peak is observed for all samples (Fig. 3A). But in reducing atmosphere, this peak is split into a sharp and a more or less broad peak. In the case of Li-V_2O_5, two sharp endothermic peaks appear (Fig. 3B).

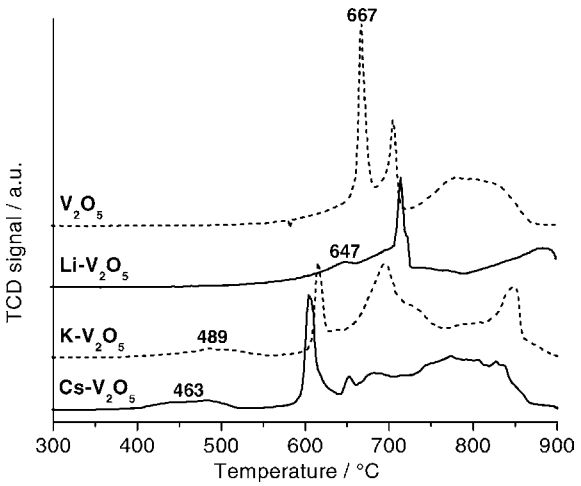

Fig. 2. TPR plots of V_2O_5, Li-V_2O_5, K-V_2O_5, and Cs-V_2O_5.

Table 2
Mass loss and temperatures of DTG and DTA peaks for the different parent catalysts calculated from the measurements in inert (He) and reducing atmosphere (5 vol.% H_2/Ar)

Catalyst	DTA (°C)		DTG (°C)		Δm (%)	
	He	H_2/Ar	He	H_2/Ar	He	H_2/Ar
V_2O_5	685	677, 715	–	668	–	2.4
Li-V_2O_5	659	671, 716	652	650	4.2	6.8
K-V_2O_5	611, 641	629, 680	610	573	3.3	8.9
Cs-V_2O_5	593, 632	620, 670	592	569	3.5	6.6

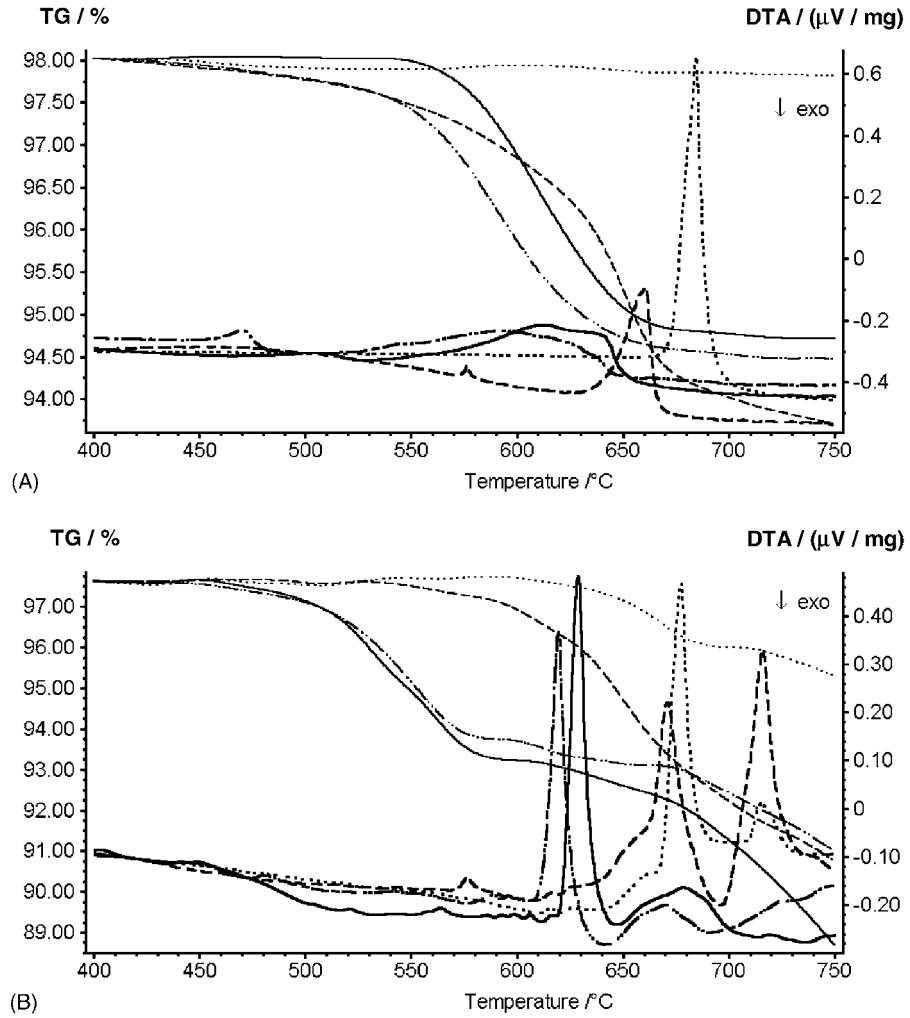

Fig. 3. TG and DTA curves of V_2O_5 (···), Li-V_2O_5 (---), K-V_2O_5 (—), and Cs-V_2O_5 (–···–) in He (A) and in 5 vol.% H_2/Ar (B).

The endothermic DTA effect for pure V_2O_5 is only slight affected by the surrounding atmosphere and is to be assigned to the melting point of V_2O_5. But, for the alkali promoted catalysts greater differences have been found, which will be elucidated later.

The reason for the mass loss in the case of the modified catalysts observed under inert and reducing atmosphere can be explained in different ways: (i) the release of SO_2 and/or H_2S originated from the incorporation of sulfate during preparation of the catalysts or (ii) the evolution of water induced by the reduction of the oxide phase.

Thermoanalytic measurements coupled with mass spectrometric analysis were carried out to investigate the composition of the evolved gases. TG curves and curves of ion current for evaluated masses measured in inert and reducing atmosphere are exemplarily presented for K-V_2O_5 in Fig. 4. The ion current curves for SO_2 (only mass number 64 is shown) and H_2S (mass number 34) are depicted. It is clearly seen that the mass loss in inert as well as in reducing atmosphere is mainly caused by the evolution of SO_2, the release of H_2S can be neglected. The release of SO_2 in reducing atmosphere is shifted to essential lower temperatures.

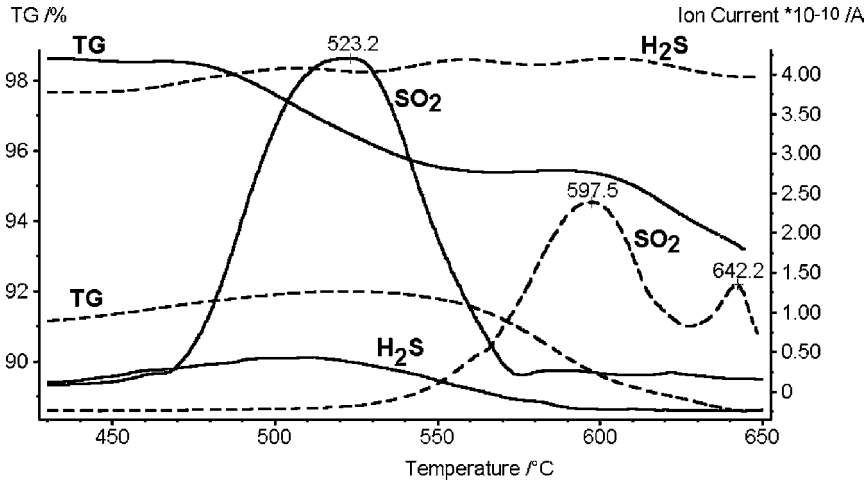

Fig. 4. TG and ion current curves of K-V_2O_5 in He (- - -) and in 5 vol.% H_2/Ar (—).

In addition to SO_2, the evolution of H_2O has been detected pointing to the beginning reduction of V_2O_5.

Kaszonyi et al. [6] have found the evolution of H_2S around 500 °C from a catalyst containing 9.3 wt.% V_2O_5, 26 wt.% K_2SO_4 and 65 wt.% SiO_2. It has to be considered, however, that the catalyst was heated in pure H_2 atmosphere. Under these conditions, the reduction of V_2O_5 starts before the evolution of H_2S. Obviously, only high H_2 concentrations in the purge gas effect the reduction of sulfate forming H_2S.

For Li-V_2O_5, a similar behaviour was found as described for the K-V_2O_5. Whereas the evolution of SO_2 proceeds in the case of K-V_2O_5 and Cs-V_2O_5 within the temperature range of 480–560 °C, a shift to 585–720 °C has been observed for Li-V_2O_5. This may point to a smaller interaction of catalyst synthesis compounds V_2O_5 and Li_2SO_4. Otherwise, it is noteworthy that the pure alkali sulphates Li_2SO_4 and K_2SO_4 do not decompose up to temperatures of 750 °C. Only the phase transition for Li_2SO_4 (monoclinic → cubic) at 577 °C was observed. This finding supports the conclusion that with the exception of Li-V_2O_5 no alkali sulfate species remain in the K-V_2O_5 and Cs-V_2O_5 catalysts. This may be an explanation for the evolution of SO_2 at relative low temperatures in the case of the K- and Cs-promoted catalysts. In H_2/Ar atmosphere, an additional lowering of the temperatures for releasing of SO_2 has been observed. Obviously, the reduction of V_2O_5 is preferred which may be accompanied by the formation of new phases. Consequently, the release of SO_2 is favoured at essential lower temperatures. To test this assumption, the change of phase composition was investigated as a function of temperature especially under reducing atmosphere. Exemplarily, the behaviour of Li-V_2O_5 and K-V_2O_5 was studied.

3.3. Changes of phase composition under reducing atmosphere: K-V_2O_5

It has been shown that in the fresh K-V_2O_5, Rb-V_2O_5, and Cs-V_2O_5 catalysts a crystalline phase MV_3O_8 was formed besides -V_2O_5. This phase could not longer be identified in samples used in the catalytic test (partial oxidation of substituted toluene) [9]. Therefore, we have prepared pure KV_3O_8 [11] to study the thermal behaviour of this phase.

The DSC curves of KV_3O_8 and of a mixture KV_3O_8/V_2O_5 (14 wt.% KV_3O_8) recorded in an Ar stream are shown in Fig. 5. The sharp endothermic effect at 496 °C corresponds to a phase transition of KV_3O_8 which is accompanied by a slight reduction indicated by the dark colour of the compound after cooling to room temperature. The XRD patterns of the compound heated up to 470 and 500 °C (before and after phase transition), respectively, are depicted in Fig. 6. Whereas after heating up to 470 °C, the pattern presents well crystalline KV_3O_8, it totally changes

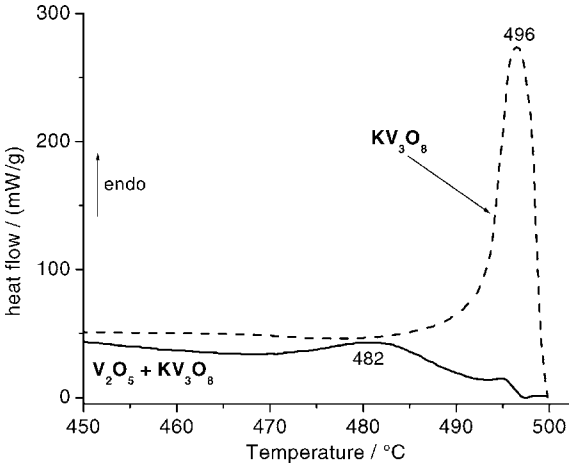

Fig. 5. DSC curves of KV_3O_8 and of 14 wt.% KV_3O_8/V_2O_5 in Ar.

after heating up to 500 °C. A new phase is formed which can be indexed with the orthorhombic cell parameters $a = 758$ pm, $b = 1181$ pm, $c = 1891$ pm. These parameters are very similar to those reported for ρ-$K_{0.5}V_2O_5$ [12,13], but with a greater cell volume. The phase ρ-$K_{0.5}V_2O_5$ possesses a bronze-like structure characterised by a mixed-valence state of vanadium.

Comparing the lattice parameters of the different KV_3O_8 phases [14] and ρ-$K_{0.5}V_2O_5$, a great similarity can be stated from the crystal geometric point of view (Scheme 1). The layer-like structures of these phases implicate a certain mobility of the potassium ions and the vanadate layers causing structural flexibility. In analogy to ρ-$K_{0.5}V_2O_5$, the orthorhombic KV_3O_8 phase obviously contains V^{4+} ions which may favour and stabilise this structure. Additionally, the dark colour of this phase points to a mixed-valence state of vanadium.

Heating a mixture of KV_3O_8 and V_2O_5 (14 wt.% KV_3O_8) up to 500 °C (see Fig. 5), only small thermal effects could be detected. No orthorhombic KV_3O_8 was formed after heating up to 500 °C. Instead $K_{0.5}V_2O_5$ and V_2O_5 have been observed as crystalline phases indicated a possible reaction or further phase transitions.

The DTA curves of K-V_2O_5 measured in He and H_2/Ar stream are depicted in Fig. 7. Considering the

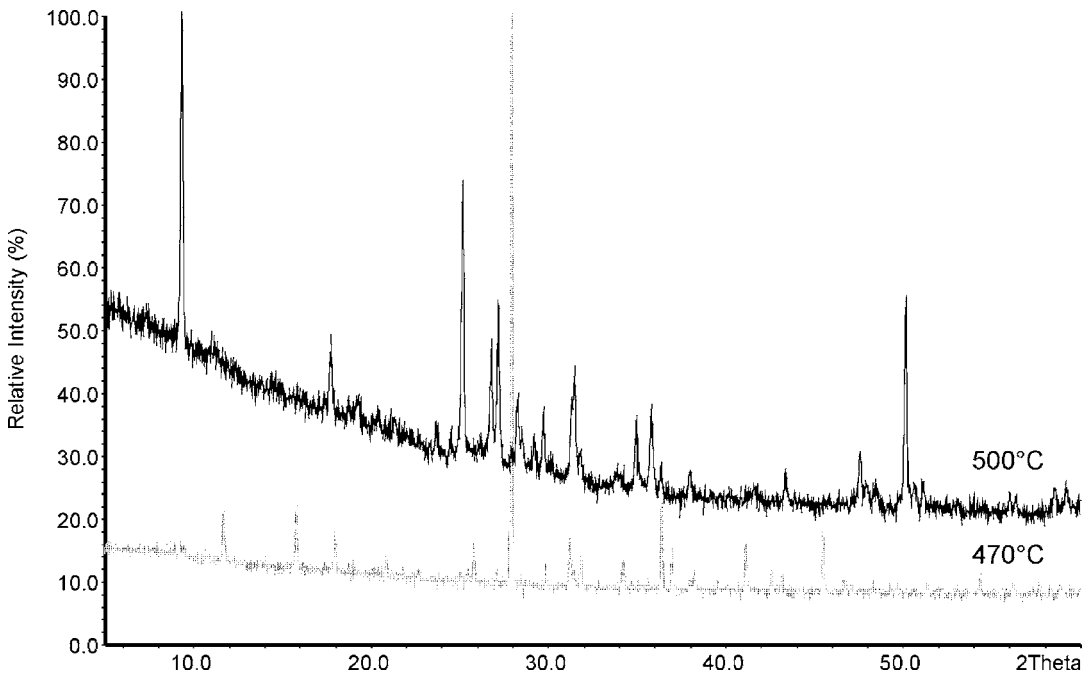

Fig. 6. XRD patterns of KV_3O_8 after heating up to 470 °C and 500 °C.

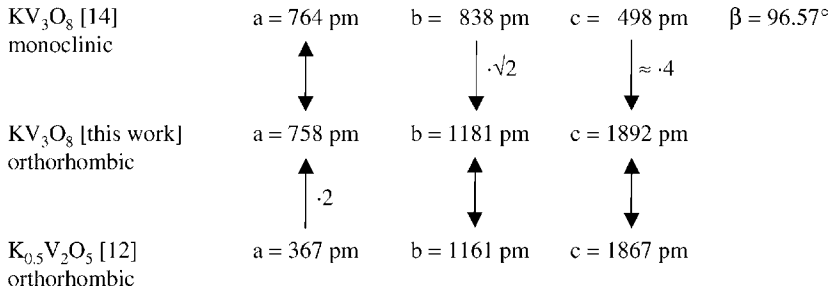

Scheme 1.

thermal behaviour of KV_3O_8, the small endothermic peak at 508 (He) and 512 °C (H_2/Ar), respectively, can be attributed to the melting and phase transition point of KV_3O_8 within the V_2O_5 matrix. K-V_2O_5 catalysts heated in He atmosphere up to 550–600 °C contain $K_{0.5}V_2O_5$ besides V_2O_5. But, after heating in reducing atmosphere up to the same temperature range, another bronze-like phase has been found.

The changes of phase composition during heating of K-V_2O_5 in H_2/Ar stream were investigated systematically. For these studies, the thermoanalytical measurement was interrupted at evaluated temperatures before and after thermal effects (cf. Fig. 7), and after cooling, the products were investigated by XRD and FTIR. The resulting XRD patterns are given in Fig. 8, the FTIR spectra are shown in Fig. 9.

At 400 °C, only V_2O_5 can be detected in the XRD pattern (cf. Fig. 8). The bands at 1201 and 1132 cm^{-1} in the respective FTIR spectrum point to incorporated sulfate ions (cf. Fig. 9). Between 545 and 600 °C, the sulfate modes vanish. This is in agreement with the release of SO_2 at temperatures above 500 °C, which was also observed by mass spectroscopic measurements as mentioned above. Within this temperature range a bronze-like phase has been formed in addition to V_2O_5 (cf. Fig. 8). The endothermic effect at 630 °C presents the melting point of these two phases (cf. Fig. 7). After melting, the reduction of the V_2O_5 phase is advanced and the pure bronze phase can be observed at 650 °C (cf. Fig. 8). This bronze phase can be indicated with monoclinic cell parameters which are very similar to the parameters described for $K_{0.23}V_2O_5$ [15] and

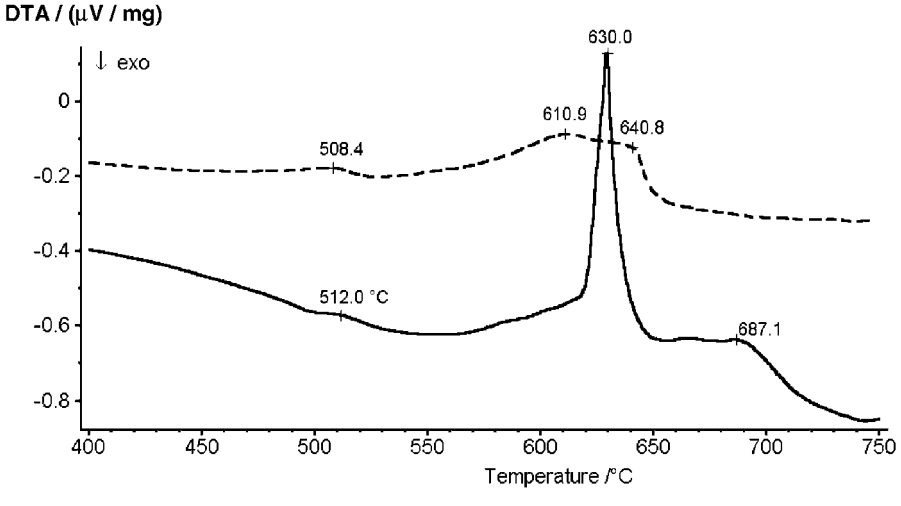

Fig. 7. DTA curves of K-V_2O_5 in He (- - -) and in 5 vol.% H_2/Ar (—).

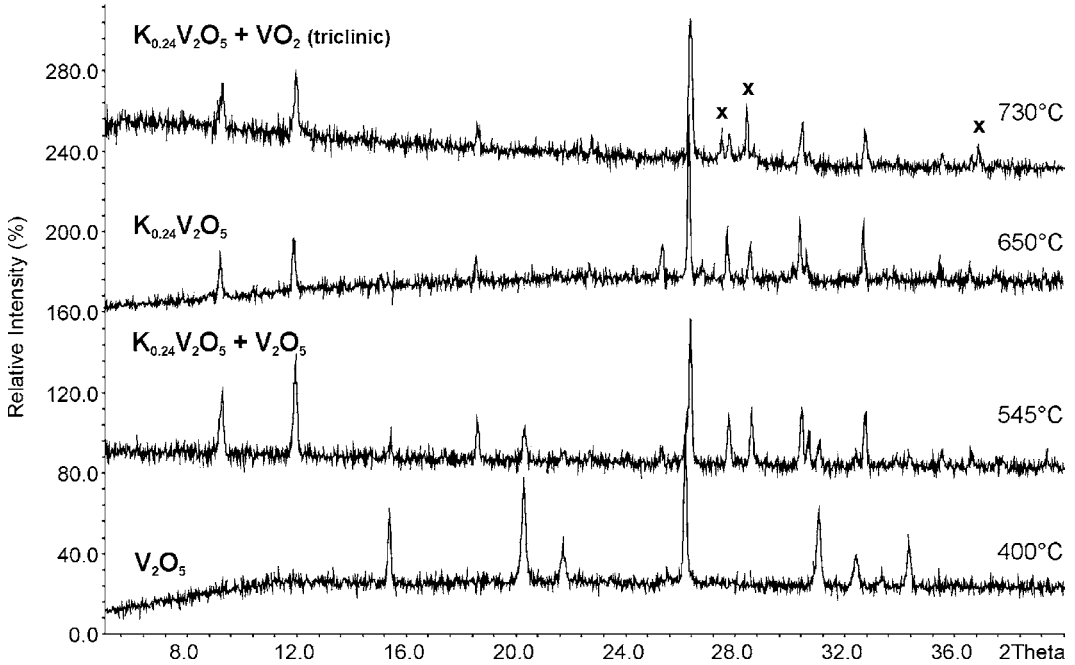

Fig. 8. XRD patterns of K-V_2O_5 after heating to 400, 545, 650, and 730 °C in 5 vol.% H_2/Ar; peaks of triclinic VO_2 are marked by ×.

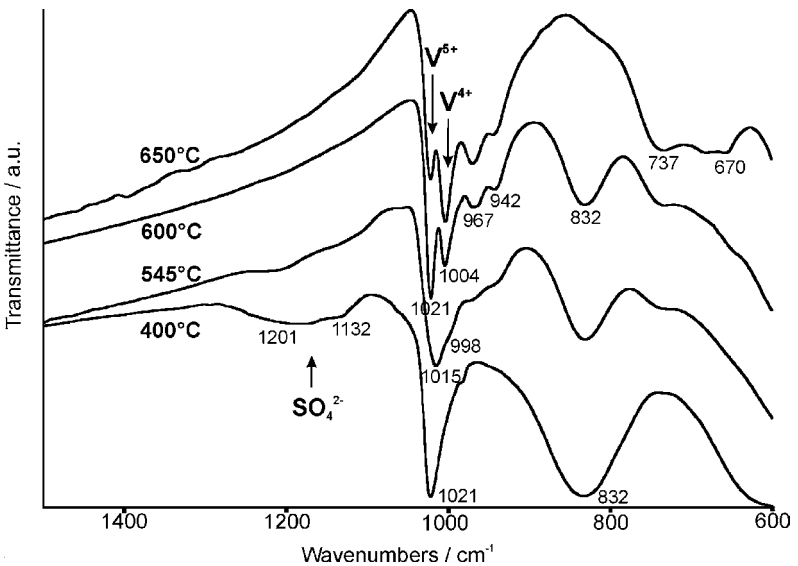

Fig. 9. FTIR spectra of K-V_2O_5 after heating to 400, 545, 600, and 650 °C in 5 vol.% H_2/Ar.

Table 3
Lattice parameters of monoclinic $K_xV_2O_5$ bronze phases

Compound	a (pm)	b (pm)	c (pm)	β (°)	V (10^6) pm^3	Reference
$K_{0.23}V_2O_5$	1012.0	360.6	1572.0	109.3	541	[15]
$K_{0.24}V_2O_5$	1010.6	361.3	1564.8	109.3	539	This work
$K_{0.25}V_2O_5$	1013.1	361.5	1574.1	109.5	544	[16]
$K_{0.33}V_2O_5$	1003.9	360.5	1533.5	109.1	524	[17]

$K_{0.25}V_2O_5$ [16]. The cell parameters of these phases and of the compound $K_{0.33}V_2O_5$ [17] which crystallises in the same space group with comparable parameters, are summarised in Table 3. It is obvious that the variation of the potassium content in this structure type is accompanied by only slight changes in lattice parameters. Considering that only crystalline phases can be detected by XRD, it is difficult to state the exact composition of the bronze phase observed in our investigations. Therefore, we have postulated the bronze to be of composition $K_{0.24}V_2O_5$ because the XRD pattern is more similar to that of the phases $K_{0.23}V_2O_5$ and $K_{0.25}V_2O_5$ than to that of $K_{0.33}V_2O_5$.

The endothermic effect around 687 °C (cf. Fig. 7) is assigned to the incongruent melting point of $K_{0.24}V_2O_5$ leading to the additional formation of triclinic VO_2 which indicates progressive reduction. The formation of the mixed valence bronze phase $K_{0.24}V_2O_5$ at 650 °C is also shown by the characteristic FTIR spectrum with the pronounced splitting of the ν(V=O) mode at 1021 and 1004 cm^{-1} (cf. Fig. 9) indicating $\nu(V^{5+}{=}O)$ with higher and $\nu(V^{4+}{=}O)$ with lower wavenumber. The typical shift of the V=O mode to lower wavenumbers points to a weakening of the V=O bond. This effect has been reported also by other authors [6,7,18,19]. Looking at the structure of the different alkali vanadium oxide bronzes, the cations are always located near the V^{5+}=O and V^{4+}=O groups [12,17] and can interact with the vanadyl groups via their dipoles.

The evolution of SO_2 at the beginning of the reduction process at about 500 °C does not influence the formation of the bronze phases. Comparative investigations of a K-V_2O_5 catalyst prepared from $KHCO_3$ instead of K_2SO_4 showed that (i) the DTA curves are identical in principle and (ii) the same products are formed at elevated temperatures. So, the reduction of the V_2O_5 is favoured and facilitates the release of SO_2.

3.4. Changes of phase composition under reducing atmosphere: Li-V_2O_5

Comparing the different thermal behaviour of K-V_2O_5 and Li-V_2O_5, the changes of phase composition during heating in H_2/Ar-stream was systematically investigated for Li-V_2O_5 too. The applied procedure was the same as described above. The thermoanalytical measurement was interrupted at elevated temperatures before and after thermal effects (Fig. 10). The resulting XRD-patterns are given in Fig. 11, the FTIR spectra are shown in Fig. 12.

After heating up to 550 °C only V_2O_5 has been detected by XRD (cf. Fig. 11). The small endothermic peak observed in inert and reducing atmosphere at 576 °C (cf. Fig. 10) corresponds to the phase transition (monoclinic → cubic) of Li_2SO_4. We have observed this peak also in an investigation of pure Li_2SO_4. Because no peaks of crystalline Li_2SO_4 were detected in the Li-V_2O_5 catalysts by XRD, an amorphous state of the lithium sulfate in the catalyst has to be assumed. Sulfate bands are clearly seen in the FTIR spectrum of the product heated up to 550 °C, but they vanish completely at temperatures above 650 °C (cf. Fig. 12).

The release of SO_2 at temperatures above 600 °C was also observed by the mass spectrometric measurements as mentioned. Accompanied by the evolution of SO_2, the reduction starts above 600 °C indicated by the formation of $Li_{0.3}V_2O_5$ which was identified an addition to V_2O_5 after heating up to 665 °C (cf. Fig. 11). The endothermic effect at 671 °C (cf. Fig. 10) represents the melting point of the mixture of $Li_{0.3}V_2O_5$ and V_2O_5. During the melting process, the reduction progresses leading to the formation of the phase $Li_{1.5}V_{12}O_{29}$. The endothermic effect around 716 °C corresponds to the incongruent melting point of $Li_{1.5}V_{12}O_{29}$ resulting in the additional formation of tetragonal VO_2 which points to further reduction.

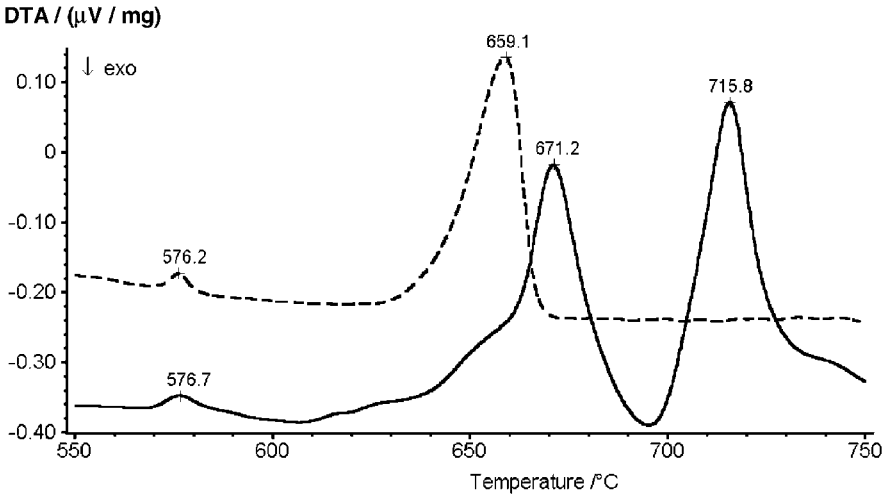

Fig. 10. DTA curves of Li-V_2O_5 in He (- - -) and in 5 vol.% H_2/Ar (—).

The phase $Li_{0.3}V_2O_5$ belongs to the same structure type as $K_{0.33}V_2O_5$ (cf. Table 3) with the monoclinic cell parameters $a = 1003$ pm, $b = 360$ pm, $c = 1538$ pm and $\beta = 110.7°$ [20]. The parameters of monoclinic $Li_{1.5}V_{12}O_{29}$ are $a = 2822$ pm, $b = 361$ pm, $c = 1012$ pm and $\beta = 102.1°$ [21]. The compound $Li_{1.5}V_{12}O_{29}$ also has a layered structure very similar to that of the other $M_{0.3}V_2O_5$ bronze phases. The FTIR spectrum of $Li_{1.5}V_{12}O_{29}$ is characterised by two bands at 983 and 932 cm^{-1} (Fig. 12). The

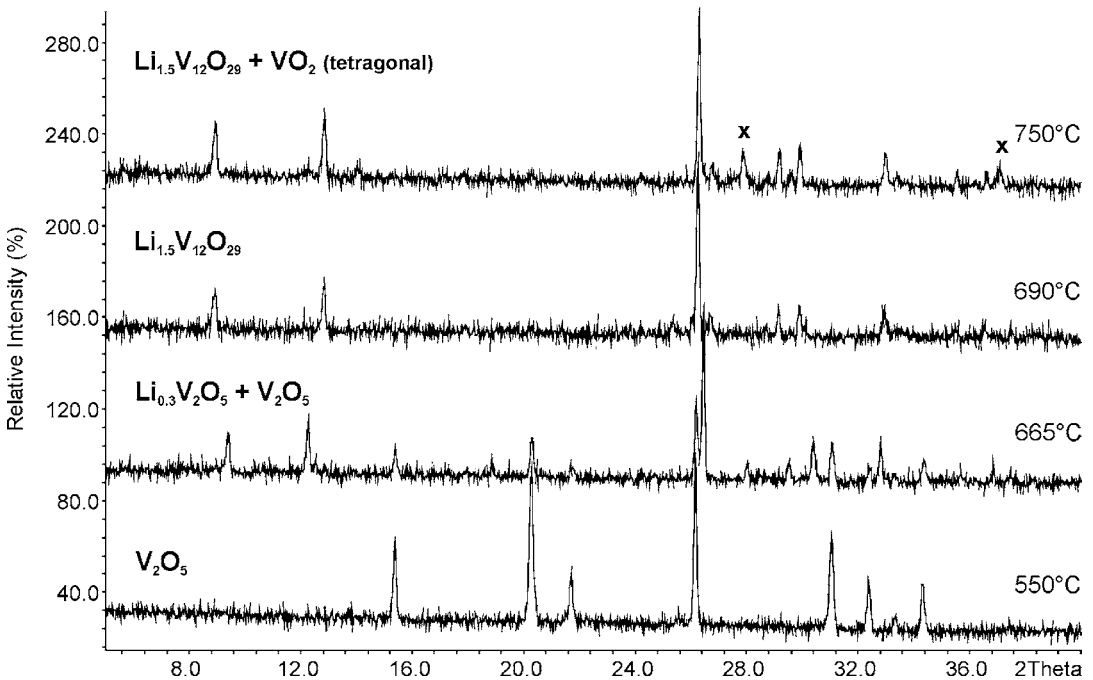

Fig. 11. XRD patterns of Li-V_2O_5 after heating to 550, 665, 690, and 750 °C in 5 vol.% H_2/Ar; peaks of tetragonal VO_2 are marked by ×.

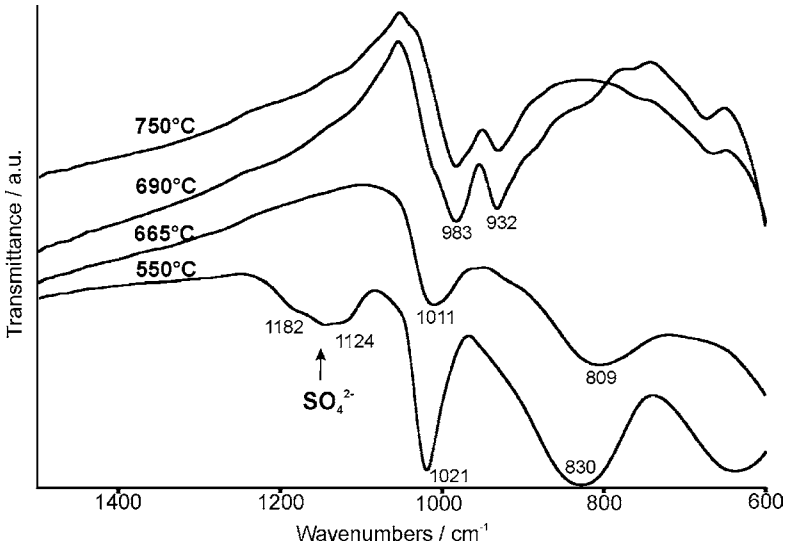

Fig. 12. FTIR spectra of Li-V_2O_5 after heating to 550, 665, 690, and 750 °C in 5 vol.% H_2/Ar.

shift of the V=O mode to lower wavenumbers is more pronounced than in the $Li_{0.3}V_2O_5$ containing product which is due to the higher portion of V^{4+} in $Li_{1.5}V_{12}O_{29}$.

4. Conclusions

From the thermoanalytical and structural point of view, the properties of Li-V_2O_5 and Na-V_2O_5 on the one hand, and of K-V_2O_5, Rb-V_2O_5, and Cs-V_2O_5 on the other hand, are very similar. Comparing the different thermal behaviour of the typical representatives K-V_2O_5 and Li-V_2O_5, it is obvious that the potassium modified V_2O_5 catalyst is reduced at essential lower temperature. The temperatures where the reduction starts decrease in the order V_2O_5 > Li-V_2O_5 ≫ K-V_2O_5 ≈ Cs-V_2O_5. That means, the reducibility is higher for K-V_2O_5 and Cs-V_2O_5 than for Li-V_2O_5, which should influence the catalytic performance in partial oxidation reactions.

The formation of crystalline mixed-valence bronze-like phases beside V_2O_5 leads to a separation of active vanadyl centres. Additionally, these bronze phases stabilise the V^{4+} oxidation state and improve the redox properties. The favoured formation of bronze-like phases especially under reducing conditions enhances the release of SO_2 at lower temperatures.

Alkali-promotion of V_2O_5 decreases the surface acidity, and therefore, the strong product adsorption is suppressed.

Acknowledgements

The authors thank Mrs. I. Kurzawski and Mrs. S. Evert for experimental assistance, Dr. H. Berndt for discussions, and the Federal Ministry of Education and Research, Germany, for financial support (project no. 03C0280).

References

[1] P.J. Gellings, H.J.M. Bouwmeester, Catal. Today 58 (2000) 1.
[2] D. Monti, A. Reller, A. Baiker, J. Catal. 93 (1985) 360.
[3] N. Shimizu, N. Saito, M. Ueshima, Successful Des. Catal. 44 (1988) 131.
[4] M. Ueshima, N. Saito, N. Shimizu, Stud. Surf. Sci. Catal. 90 (1994) 59.
[5] M. Ponzi, C. Duschatzky, A. Carrascull, E. Ponzi, Appl. Catal. A 169 (1998) 373.
[6] A. Kaszonyi, M. Hronec, G. Delahay, D. Ballivet-Tkatchenko, Appl. Catal. A 184 (1999) 103.

[7] T. Ono, Y. Tanaka, T. Takeuchi, K. Yamamoto, J. Mol. Catal. A 159 (2000) 293.
[8] D.A. Bulushev, L. Kiwi-Minsker, V.I. Zaikovskii, O.B. Lapina, A.A. Ivanov, S.I. Reshetnikov, A. Renken, Appl. Catal. A 202 (2000) 243.
[9] A. Martin, U. Bentrup, G.-U. Wolf, Appl. Catal. A 227 (2002) 131.
[10] K. Tarama, S. Teranishi, S. Yashida, N. Tamura, in: Proceedings of the Third International Congress on Catalysis, Vol. I, Amsterdam, 1964, p. 282, North Holland Amsterdam, 1965.
[11] A.D. Kelmers, J. Inorg. Nucl. Chem. 21 (1961) 45.
[12] J.-M. Savariault, J. Galy, J. Solid State Chem. 101 (1992) 119.
[13] Y. Kanke, K. Kato, E. Takayama-Muromachi, M. Isobe, K. Kosuda, Acta Cryst. C46 (1990) 1590.
[14] H.T. Evans, S. Block, Inorg. Chem. 5 (1966) 1808.
[15] J. Van den Berg, Phys. Chem. Miner. 87 (1983) 120.
[16] M.T. Vandenborre, C. Sanchez, A. Politi, Nouv. J. Chim. 9 (1985) 511.
[17] R.P. Ozerov, G.A. Golder, G.S. Zhdanov, Kristallografiya 2 (1957) 217.
[18] G. Ramis, G. Busca, F. Bregani, Catal. Lett. 18 (1993) 299.
[19] G. Deo, I.E. Wachs, J. Catal. 146 (1994) 335.
[20] A. Hardy, J. Galy, A. Casalot, M. Pouchard, Bull. Soc. Chim. Fresenius (1965) 1056.
[21] K. Kato, E. Takayama-Muromachi, Acta Cryst. C43 (1987) 1447.